ground water

Inverse Modeling of Coastal Aquifers Using Tidal Response and Hydraulic Tests

by Andrés Alcolea[1], Eduardo Castro[2], Manuela Barbieri[2], Jesús Carrera[3], and Sergio Bea[3]

Abstract

Remediation of contaminated aquifers demands a reliable characterization of hydraulic connectivity patterns. Hydraulic diffusivity is possibly the best indicator of connectivity. It can be derived using the tidal response method (TRM), which is based on fitting observations to a closed-form solution. Unfortunately, the conventional TRM assumes homogeneity. The objective of this study was to overcome this limitation and use tidal response to identify preferential flowpaths. Additionally, the procedure requires joint inversion with hydraulic test data. These provide further information on connectivity and are needed to resolve diffusivity into transmissivity and storage coefficient. Spatial variability is characterized using the regularized pilot points method. Actual application may be complicated by the need to filter tidal effects from the response to pumping and by the need to deal with different types of data, which we have addressed using maximum likelihood methods. Application to a contaminated artificial coastal fill leads to flowpaths that are consistent with the materials used during construction and to solute transport predictions that compare well with observations. We conclude that tidal response can be used to identify connectivity patterns. As such, it should be useful when designing measures to control sea water intrusion.

Introduction

The original motivation for this study was to characterize a contaminated site near the coast in eastern Spain. Design of remediation measures requires identifying preferential flowpaths (i.e., connectivity patterns) in the study area. In fact, characterizing sea aquifer connectivity is often needed for coastal aquifer management. For example, Abarca et al. (2006) found that fresh water injection along a hydraulic barrier to control sea water intrusion should concentrate along a paleochannel connecting the aquifer with the sea. Knudby and Carrera (2005) showed that hydraulic diffusivity "D" ($D = T/S$, where T and S are transmissivity and storage coefficient, respectively) is possibly the best indicator of hydraulic connectivity. Therefore, one would expect that characterization methods leading to reliable estimations of diffusivity should also contain valuable information about connectivity of high–hydraulic conductivity paths. Since tides can be viewed as large-scale aquifer tests, they provide large-scale information on aquifer diffusivity. In fact, point values of effective hydraulic diffusivity "D_{eff}" are easily obtained from the interpretation of tidal response at a borehole (Erskine 1991; Schultz and Ruppel 2002; Jhan et al. 2003; Fakir 2003; Shih and Lin 2004; Trefry and Bekele 2004). The tidal response method (TRM) estimates D_{eff} from the amplitude and/or the time lag of the tidal response at an observation borehole (Ferris 1951; Hvorslev 1951). This analytical solution assumes a one-dimensional flow in a homogeneous and infinite confined aquifer, which is subjected to a sinusoidal perturbation at its boundary (assumed vertical). Estimated D_{eff} is often validated in parallel with the interpretation of hydraulic tests (Drogue et al. 1984; Millham and Howes 1995).

Efforts have been devoted to relaxing the TRM assumptions. Li et al. (2002) present an analytical solution in a confined and L-shaped aquifer, extending the solution to

[1]Corresponding author: School of Civil Engineering, Universitat Politecnica de Catalunya, Jordi Girona st. 1-3. 08034, Barcelona, Spain. Currently at CHYN, Centre of Hydrogeology, University of Neuchâtel, rue Emile Argand, 11, E318, CP 158, CH-2009, Neuchâtel, Switzerland; +41 32 718 2597.

[2]School of Civil Engineering, Universitat Politecnica de Catalunya, Jordi Girona st. 1-3. 08034, Barcelona, Spain; + 34 93 401 6890; fax +34 93 401 7251.

[3]Institut de Ciencias de la Terra, Consejo Superior de Investigaciones Cientificas. Lluis Sole Safaris st n/n, 08028, Barcelona, Spain; +34 93 409 5410; fax +34 93 411 1112.

Received November 2006, accepted May 2007.

doi: 10.1111/j.1745-6584.2007.00356.x

leaky aquifers (Li and Jiao 2001). Anisotropy of hydraulic conductivity is assessed by Pandit et al. (1991). One-dimensional modeling of tidal propagation in a coastal aquifer with complex heterogeneity is explored by Trefry (1999). The effect of boundary heads representing tidal fluctuations is studied by Wang and Tsay (2001) and Jhan et al. (2003), who use a superposition of harmonics.

Estimating D_{eff} by the TRM and complementing it with hydraulic tests suffers from a number of difficulties. First, TRM yields point values of D_{eff}, but does not acknowledge heterogeneity, which may affect the aquifer response to tides. Second, hydraulic test data may not be suitable for standard analysis due to the superposition of pumping and tidal effects (Trefry and Johnston 1998; Chen and Jiao 1999). TRM can be used for filtering the tidal effects but requires a known hydraulic diffusivity. An additional shortcoming is that TRM does not represent real tide accurately (sinus function in the study of Chapuis et al. [2006] or a superposition of harmonics, Wang and Tsay [2001]; Jhan et al. [2003]).

We conjecture that geostatistical inversion may allow us to overcome the aforementioned drawbacks. First, strict assumptions of the TRM are relaxed. For instance, complex model geometries and heterogeneities can be accommodated. Second, joint interpretation of tidal response at all boreholes of the observation network should yield the connectivity structure rather than a set of point values of diffusivity. Third, explicit numerical modeling of tidal fluctuation enables us to accommodate observed fluctuations of sea level, which contain both deterministic and random components. Fourth, numerical inversion facilitates explicit incorporation of hydraulic test data. This should not only improve the identification of connectivity patterns (Carrera and Neuman 1986c; Meier et al. 1998; Weiss and Smith 1998) but also allow us to resolve diffusivity into transmissivity and storage coefficient (Carrera and Neuman 1986b; Rötting et al. 2006).

The objective of this study was to test the aforementioned conjecture. We present a procedure to integrate tidal response and injection test data so as to characterize connectivity patterns at coastal aquifers. The procedure is based on the regularized pilot points method (Alcolea et al. 2006a, 2006b). The method is applied to a polluted site that consists largely of an artificial fill. This allows us to compare "as-built" maps with preferential flowpaths derived from inversion.

Site Description

The polluted site under study was occupied by a factory. The ultimate objective of this study was to characterize the study area to identify potential migration paths and design a remediation system. The study area (Figure 1) is located at the edge of an unconfined coastal aquifer. It is made up of an anthropogenic fill lying on top of Quaternary conglomerates (zone 1). The anthropogenic fill consists of several zones (zones 2 through 7 in Figure 1) where different materials were deposited down to 10 m deep. The mean depth of the water table is 5 m. Thus, zones with a saturated thickness of around 5 m, some filled with highly conductive material, can be found. These zones become preferential flowpaths.

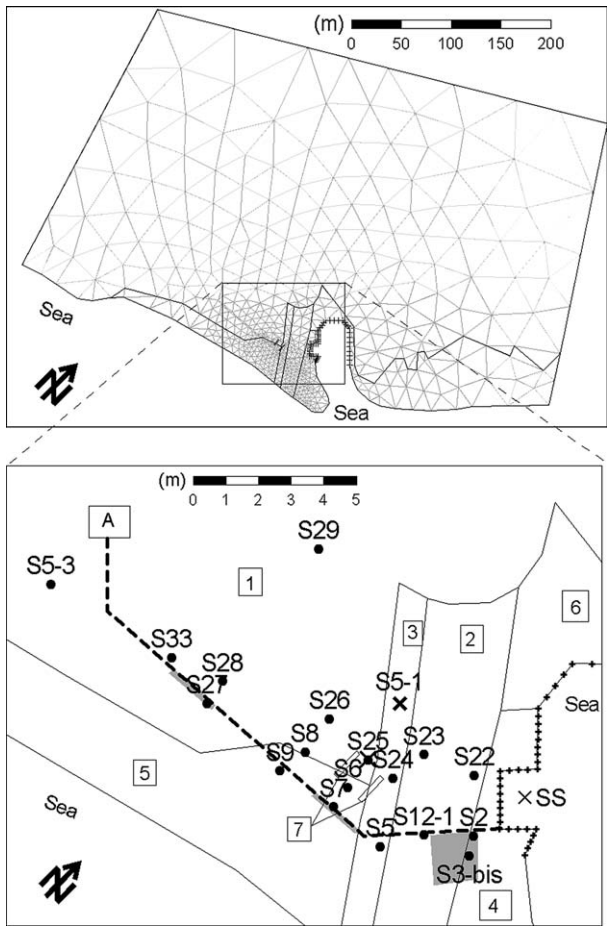

Figure 1. Site description state. The study area (below) lays on top of a Quaternary conglomerate (zone 1). Zone 2 accommodates two pipelines for sea water pumping. Zone 3 was dug to accommodate these pipelines. Zones 4 through 6 represent land gained to the sea, covered with tetrapod marine defenses. They cover the seashore except in its middle part (depicted by crosses), where a concrete wall panel was built for protection. Zones indicated by "7" are concrete structures that cover almost the whole saturated thickness. Contamination has been detected in the three shaded zones, where the discharge pipeline (dashed line) was presumably broken. Observation boreholes are depicted by black circles.

A review of the factory construction project reveals an approximate location of zones of anthropogenic heterogeneity (Figure 1):

- Sea water pipelines (zone 2). An underground concrete structure (3.5 m thick) is located on top of the conglomerate base in this zone. This structure contains sea water pipelines and was covered with a gravel fill. While the structure reduces the saturated thickness, which is approximately 1 m in this zone, large transmissivity values are expected.
- Sea water pipelines filling (zone 3). Conglomerates in zones 2 and 3 were dug to accommodate the sea water pipelines. Thereafter, anthropogenic material was used to fill up this excavation. Presumably, this highly conductive material and the elongated shape of this zone render it the most suitable preferential flowpath.
- Land gained to the sea (zones 4 through 6). The conglomerate base in these areas is covered with granular fill

and tetrapod marine defenses. These structures protected the factory from the sea. A concrete wall panel protected the factory in the middle part of the shore (depicted by crosses in Figure 1). Presumably, this wall covers almost the whole saturated thickness.

- A discharge pipeline (dashed line in Figure 1) was placed in the unsaturated zone of the aquifer. Two concrete structures (zone 7) were built to support this pipeline. The construction project reveals that these structures cover the whole saturated thickness.

Prior fieldwork in the study area detected contamination in the shaded zones of Figure 1. Presumably, the discharge pipeline was broken in these zones. Although prior studies estimated that the breach occurred in 1975, it was not detected until 1992. Thus, the contaminant spilled and accumulated in the unsaturated zone for a long time. The proposed remediation system consists of the recharge of brackish water, which will shift the pollutant toward the saturated zone. Pumping at selected locations will remove it from the aquifer, thus avoiding a spill to the sea. Selection of the pumping scheme (location of pumping wells, pumping rates, etc.) demands a prior characterization of the study area in terms of hydraulic and preferential flowpaths, which motivates the development of our methodology.

Methodology

Tidal Fluctuation Response

Absolute pressure was automatically recorded at the seashore (sensor SS in Figure 1) and at 20 boreholes using TD-Diver (Van Essen Instruments, Schlumberger, Delft, The Netherlands). These measurements were transformed into relative pressures by subtracting barometric pressure (measured at borehole S22 using Baro-Diver, Van Essen Instruments, Schlumberger). Next, heads were obtained as the sum of pressure head and diver elevation.

The very high-frequency fluctuations of sea level (i.e., due to wind and waves) were filtered out as they are assumed not to propagate far within the aquifer. To simplify boundary and initial conditions, we express tidal response in terms of variations with respect to natural heads. Thus, we only need to simulate head changes induced by sea-level fluctuations but not the regional flow in the aquifer. To this end, head measurements at every borehole were corrected by subtracting their mean value.

Unbiasedness in the calculation of mean head at a borehole requires a long measurement period. This long record was not available at most boreholes due to low availability of pressure sensors (only boreholes S5, S9, and SS were continuously monitored during 41 d). In addition, measured heads during injection periods were suppressed as tidal and injection effects were superimposed. We used kriging with external drift for filling these gaps (lack of monitoring and injection periods) using the records at boreholes S5 and S9 (not affected by injections) as external drifts. The resulting reconstructed record at every borehole was used to compute mean head. This mean was then subtracted from the actual measurements to obtain the tidal fluctuations that are actually used in calibrating the model. The procedure is outlined in the Appendix.

Hydraulic Tests

Hydraulic tests data provide further information on connectivity and are needed to resolve diffusivity (outcome when only the tidal fluctuation response is analyzed) into transmissivity and storage coefficient. Two injection tests were performed in the area of interest. Relevant data about these tests are summarized in Table 1. Even though injection rates were very high, the observed response to injections at monitored boreholes reached a maximum of only 4 cm. Thus, it was masked by tidal effects (amplitude of tide is ~40 cm). Reconstruction of head evolution during injection periods, as described in the previous section, allows us to filter the tidal effect. Simply, we subtract the kriged values (in response to tidal effect) from the actual measured heads (Figures 2 and 3).

Available measurements of T and S (Table 2) arise from a preliminary interpretation of a set of hydraulic tests that had been performed during a previous study. The code EPHEBO (UPC 2002) was used to this end. Estimated storage coefficients were about 0.1 for the Quaternary conglomerates and 0.3 for the anthropogenic fill in most cases. Estimated transmissivities ranged from 15 to 350 m^2/d for the conglomerates. Analysis of data at boreholes S12-1 (sea water pipeline) and S24 (sea water pipeline filling) yields transmissivities of 150 and 225 m^2/d, respectively. However, this interpretation displayed a large uncertainty (i.e., large confidence intervals in the estimation). We attribute this to the fact that all boreholes are partially penetrating (few centimeters in the saturated zone), which may lead to an underestimation of transmissivity values.

Table 1
Description of Injection Tests in the Study Area

	Injection Type	Injection Rate (m^3/d)	Injection Interval (d)	Total Injection Volume (m^3)	Recovery Period (d)	Available Measurements
Injection at S5-1	In two steps	199	0–0.26, 0.46–0.90	198	0.90–1.40	S5, S6, S9 (no response); S12-1, S24, S25, S26, S29
Injection at S25	Continuous	130	0–0.5	66	0.5–1.05	S5, S7, S8, S9 S26, S29 (no response); S24

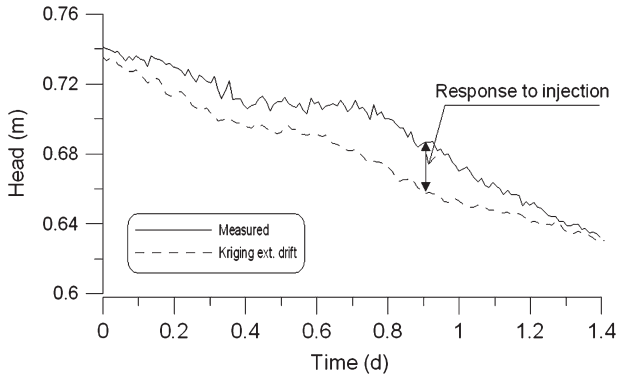

Figure 2. Kriged and measured heads at borehole S12-1 during injection test 1 at borehole S5-1.

Table 2
Available Transmissivity Measurements in the Study Area

Zone	Borehole	Transmissivity (m^2/d)
Quaternary conglomerate (zone 1)	S7	75
	S8	25
	S25	15
	S28	350
	S29	50
Sea water pipeline (zone 2)	S12-1	150
Sea water pipeline filling (zone 3)	S24	225

Note: This information arises from the standard analysis (e.g., homogeneous medium) of available hydraulic tests.

Model Calibration

Inversion methodology follows roughly the procedure described by Meier et al. (2001) and Rötting et al. (2006) to identify preferential flowpaths. The main differences stem from (1) the use of the regularized pilot points method (Alcolea et al. 2006a); (2) the use of tidal response data; and (3) the anthropogenic nature of the site. The latter allows us to compare the flowpaths obtained using only hydraulic data to those revealed by construction records.

The regularized pilot points method parameterizes a hydraulic property (typically $\log_{10} T$) as the sum of a deterministic drift and an unknown residual. The drift is calculated by conditional estimation (ordinary kriging with measurement error in this case) to available direct measurements, if any, assuming a known correlation structure defined by a variogram. The residual can be viewed as the perturbation needed by the drift to honor measurements of dependent variables (heads, concentrations, etc.). The optimum set of model parameters (value of the hydraulic property at the pilot point locations depicted in Figure 4) minimizes an objective function F, which accounts for matching measurements of dependent variables and parameter plausibility:

$$F = \sum_{i=1}^{\text{nstat}} (\mathbf{u}_i(\mathbf{p}) - \mathbf{u}_i^*)^t \mathbf{V}_{\mathbf{u}_i}^{-1} (\mathbf{u}_i(\mathbf{p}) - \mathbf{u}_i^*) + \sum_{j=1}^{\text{ntypar}} \mu_j (\mathbf{p}_j - \mathbf{p}_j^*)^t \mathbf{V}_{\mathbf{p}_j}^{-1} (\mathbf{p}_j - \mathbf{p}_j^*) \quad (1)$$

where "nstat" denotes number of types of state variables $\mathbf{u}_i$ with available measurements $\mathbf{u}_i^*$ and covariance matrix $\mathbf{V}_{\mathbf{u}_i}$. In this case, two subsets of state variables were used

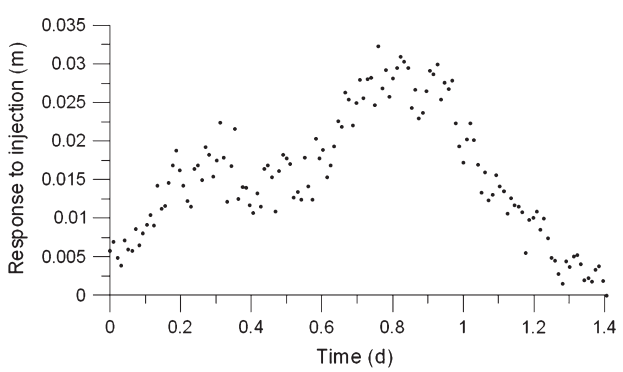

Figure 3. Filtered response to injection test 1 at borehole S12-1.

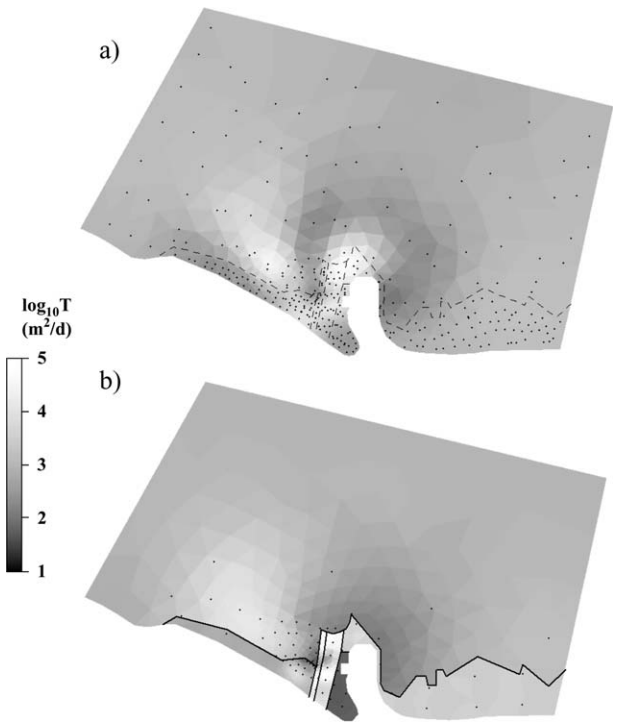

Figure 4. Estimated log-transmissivities using tidal response and injection tests as calibration data. (a) Hydraulic information–based model (i.e., zonation not accounted for explicitly). (b) Geology-based model. Lines depict the contact between anthropogenic zones (dashed for the hydraulic information-based model as they are not accounted for). Pilot points are depicted by dots.

($i = 1$ for tidal responses and $i = 2$ for injection test data). After Carrera and Neuman (1986a), we assumed $\mathbf{V}_{\mathbf{u}_i}$ to be diagonal ($\mathbf{V}_{\mathbf{u}_i} = \sigma^2_{\mathbf{u}_i}\mathbf{I}$, where $\sigma_{\mathbf{u}_i}$ is the unknown standard deviation of the error in the corresponding measurement type and $\mathbf{I}$ is the identity matrix). "ntypar" is the number of types of model parameters $\mathbf{p}_j$ being calibrated (organized in vector $\mathbf{p}$), with prior information $\mathbf{p}_j^*$ and covariance matrix $\mathbf{V}_{\mathbf{p}_j}$ (in this case, $j = 1$ for pilot points related to transmissivity, $j = 2$ for those of storage coefficient, etc.). $\mathbf{V}_{\mathbf{p}_j}$ is the kriging error covariance matrix. $\mathbf{p}_j^*$ is calculated in the same way as the deterministic drift. μ_j are weighting scalars correcting errors in the specification of the covariance matrices (see, e.g., Carrera and Neuman [1986a] for a discussion on the statistical meaning of μ_j).

Two model structures are used for representing the relationship between dependent variables $\mathbf{u}$ and model parameters $\mathbf{p}$. They differ in the specification of the geological zonation. First, we neglected such information, so that actual patterns of connectivity (as revealed by the construction project) were ignored. This first model structure is termed "hydraulic information-based model" hereinafter. Second, this information was explicitly stated in the model ("geology-based model"). For the latter, heterogeneity of $\log_{10} T$ field in each zone was defined by an isotropic spherical variogram. The ranges were 50 and 25 m for the conglomerates and for the zones of anthropogenic heterogeneity, respectively. Corresponding sills were 1 and 0.5 (i.e., $\log_{10} T$ can vary 1 order of magnitude—or half an order—within a correlation range). When the geological zonation was ignored, a single transmissivity zone encompassed the whole model domain. In this case, the variogram is spherical with range 50 m and a sill of 1. The few (and uncertain) $\log_{10} T$ available measurements complicated the specification of the aforementioned variograms. This affects the calculations of $\mathbf{p}_j^*$ and the corresponding covariance matrices and will be discussed later. Prior interpretation of hydraulic tests (Table 2) yielded almost constant values of storage coefficient for the conglomerates and for the anthropogenic fill. Thus, regardless of the zonation of transmissivity, we assumed the storage coefficient to be constant (modeled by a single pilot point), but unknown, in these zones.

Both hydraulic information-based and geology-based models share the same boundary and initial conditions. These were homogeneous (i.e., zero head variations and fluxes) because we seek head variations. Only the boundary conditions governing the test (i.e., sea-level fluctuation for tidal response and flow rates for the injection tests) must be expressed as time functions. All other boundary conditions are zero. Likewise, areal recharge does not need to be evaluated. The concrete wall in the middle part of the seashore (depicted by crosses in Figure 1 connecting zones 4 and 6) is modeled by a mixed boundary condition. The leakage coefficient was assumed to be constant and known (~10^{-7}/d). This small value led to a negligible flux through the wall panel as it was assumed to cover almost the whole saturated thickness. Boundary conditions for the three tests interpreted are summarized in Table 3. Initial head variations are also zero given that, before the start of the test, heads are defined by "natural" conditions of the system.

A two-dimensional finite-element mesh of 1039 elements (Figure 1) was used. Element size increases as the mesh progresses outside the area of interest. This area was enlarged to identify preferential flowpaths, so as to ascertain the extent of the pollutant plume, and to avoid spurious boundary effects. Forward in time finite differences were used to model temporal behavior. The time step was 0.01 d (15 min). This was chosen equal to the frequency of sampling. Simulation times span the intervals [0, 20.8], [0, 1.4], and [0, 0.9] (units in days) for tidal response and for injections at S5-1 and S25, respectively.

Three sources of information were included as conditioning data. On the one hand, hydraulic data arising from tidal response and from injection tests were analyzed simultaneously. Available measurements of T and S (Table 2) were used to calculate prior information of the model parameters. Due to the large uncertainty of these measurements, a variance of 3 (log scale) was assigned to each measurement. The key point of the inversion methodology is the specification of the statistical parameters in Equation 1. The statistical unknowns are (σ_1, σ_2), the standard deviations of tidal response and injection test data, respectively, and (μ_1, μ_2), the weights of the plausibility terms of $\log_{10} T$ and $\log_{10} S$, respectively. Optimum

Table 3
Summary of Boundary Conditions of the Flow Characterization Model

Boundary	Type	Problem 1 Tidal Response	Problem 2 Injection at S5-1	Problem 3 Injection at S25
Left	Prescribed flow	$Q = 0$	$Q = 0$	$Q = 0$
Right	Prescribed flow	$Q = 0$	$Q = 0$	$Q = 0$
Upper	Prescribed flow	$Q = 0$	$Q = 0$	$Q = 0$
Seashore	Prescribed head	$\Delta h = \Delta H_{sea}$	$\Delta h = 0$	$\Delta h = 0$
Middle part of the seashore (concrete wall panel)	Mixed	$Q = \alpha\,(\Delta H_{sea} - \Delta h)$	$Q = \alpha\,(0 - \Delta h)$	$Q = \alpha\,(0 - \Delta h)$
S5-1	Prescribed flow	—	$Q = f(t)$[1]	—
S25	Prescribed flow	—	—	$Q = 130$ m^3/d

[1] $f(t)$ denotes the variable injection rate at borehole S5-1, as described in Table 2.

values of statistical parameters maximize the expected likelihood of the parameters given the data (Medina and Carrera 2003).

Transport Prediction

Estimated $\log_{10} T$ fields and $\log_{10} S$ were validated in the prediction of a transport model. This is aimed at reproducing the movement of the contaminating solute under "natural" steady-state flow conditions. "Natural" flow conditions consist of prescribing no flow along the left and right boundaries (they represent regional streamlines), a prescribed flow along the upper boundary simulating regional flow, and a prescribed head on the seashore simulating mean sea level (zero). A constant mass flux is prescribed along the upper boundary (regional flow times background concentration). The contaminating episode was modeled by prescribing mass fluxes in the contaminated areas (shaded zones in Figure 1). These fluxes were the outcomes of a reactive transport model (Bea et al. 2004) simulating the mobilization of the solute from the unsaturated zone to the saturated one. The main uncertainties of that model were the exact position of the breaks in the discharge pipeline and its leakage, which control the boundary conditions and, consequently, the output (i.e., source terms in our transport model). A constant initial concentration representing the background concentration ($c = 30$ Bq/m^3, where Bq denotes Becquerel) is prescribed over the whole domain. Flow and transport boundary conditions and parameters are summarized in Table 4. A sensitivity analysis to dispersivities and retardation factors was performed, being the model more sensitive to the latter. A geology-based zonation for the retardation factor was chosen, assigning a percentage of clay to each material. We calculated the retardation factor from that percentage using a cation exchange model. The geometry of the model remains unaltered. However, the finite-element mesh was refined to avoid numerical dispersion (16,624 elements). The contaminating solute was measured at boreholes S2, S3-bis, S5, S8, S12-1, S23, S24, S25, S26, S27, and S28.

Results

Results are evaluated in terms of estimation plausibility and fits of measured state variables (head variations and concentrations). $\text{Log}_{10} T$ fields obtained by the hydraulic information–based and geology-based models are depicted in Figure 4. Fits of measured head variations are presented in Figure 5 (tidal response) and Figure 6 (injection data). Only fits of the hydraulic information–based model are presented given that the ones using the geology-based model are very similar. State variable residuals are summarized in Table 5. A quantitative comparison of $\log_{10} T$ fields obtained by both models is summarized in Table 6. Results of transport prediction are displayed in Figure 7.

Assigning proper weights to the different data sets is an important aspect of the inversion methodology. Weighting is controlled by the statistical parameters in Equation 1, which control the contribution of each data set in the calibration process. For instance, if the standard deviation of tidal response data (σ_1) is small compared to the standard deviation of injection test data (σ_2), the large volume of tidal response data may dominate the objective function F, thus hindering the information contained in data arising from injections and vice versa. Likewise,

Table 4
Summary of Boundary Conditions and Parameters of the Transport Model

Zone	Equation	Type	Value
Left boundary	Flow	Prescribed flow	$Q = 0$ m^3/d
Right boundary	Flow	Prescribed flow	$Q = 0$ m^3/d
Upper boundary	Flow	Prescribed flow	$Q = 2.19$ m^3/d
	Transport	Mass flux	$c = 30$ Bq/m^3
Lower boundary	Flow	Prescribed head	$H = 0$ m
Contaminated zones	Flow	Prescribed flow	$Q = 0.73$ m^3/d
	Transport	Mass flux	$c = f(t)$ Bq/m^3
Whole domain	Flow	Areal recharge	$q_r = 2.7 \times 10^{-4}$ mm/d
	Transport	Mass flux	$c = 30$ Bq/m^3
Concrete wall	Flow	Leakage	$\alpha = 1 \times 10^{-7}$d^{-1}; $H = 0$ m
Longitudinal dispersivity	Transport	—	3 m
Transverse dispersivity	Transport	—	0.3 m
Porosity	Transport	—	0.2 m
Saturated thickness	Transport	—	2.5 m
Retardation coefficient (zone 1)	Transport	—	250
Retardation coefficient (zone 2)	Transport	—	80
Retardation coefficient (zone 3)	Transport	—	80
Retardation coefficient (zone 4)	Transport	—	60
Retardation coefficient (zone 5)	Transport	—	100
Retardation coefficient (zone 6)	Transport	—	100

Notes: $f(t)$ denotes the time function simulating the mass of solute flowing from the unsaturated zone toward the saturated zone. This arises from a reactive transport model.

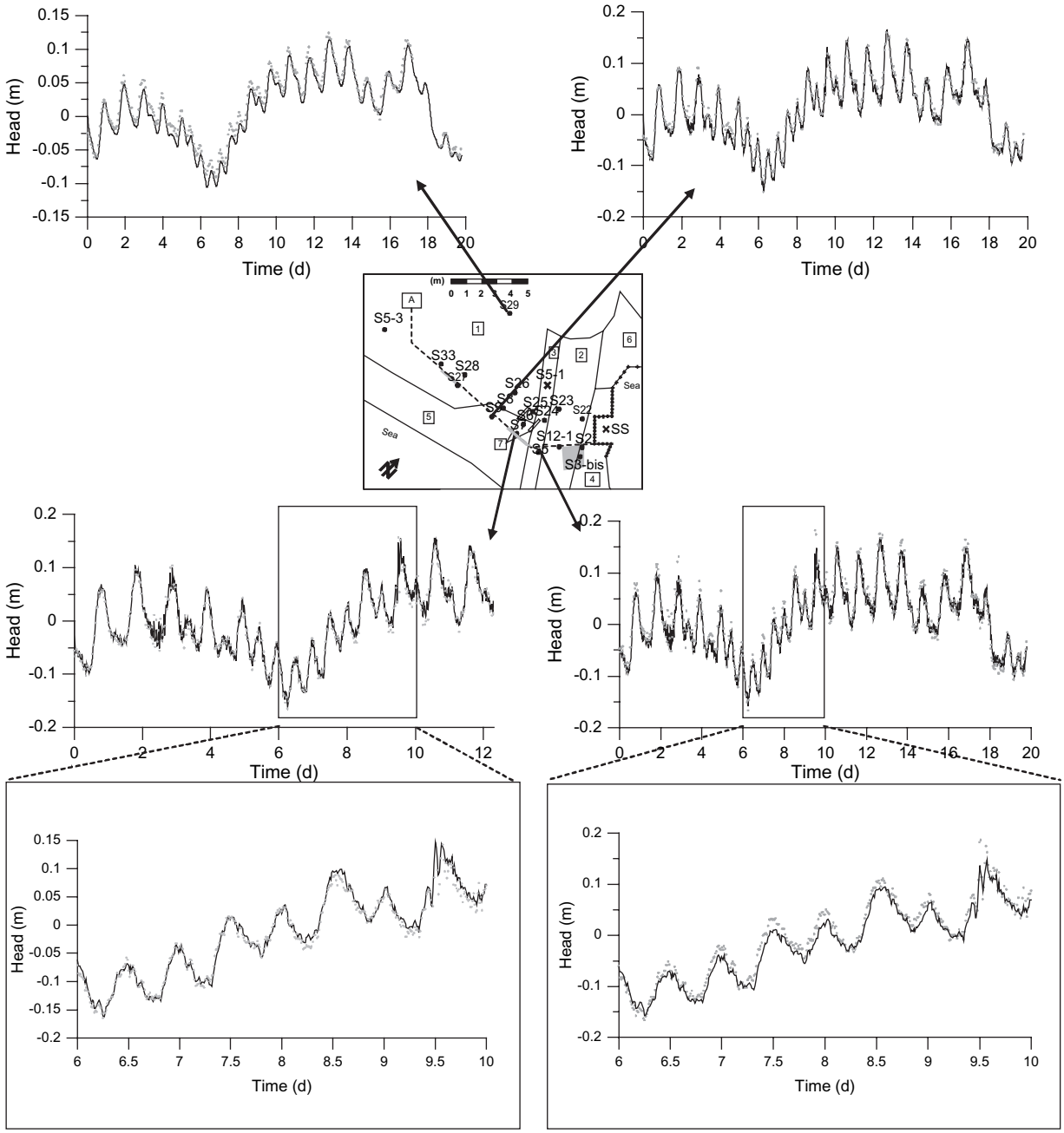

Figure 5. Calculated (lines) vs. measured (circles) tidal response vs. time using $\log_{10} T$ field calibrated by the hydraulic information-based model (Figure 4a).

assigning large plausibility weights biases the solution toward the deterministic drift (Alcolea et al. 2006a), which in this case was poorly informative, due to the large uncertainty of available direct measurements. On the contrary, assigning small weights leads to the best match of dependent variables but also to an unstable characterization of the unknown properties. Fortunately, framing the regularized pilot points method in a maximum likelihood context allows us to obtain the optimum values of the statistical parameters. These maximize the expected likelihood of the parameters given the data (Medina and Carrera 2003). Thirty-six calibration runs were performed, with values of 0.5×10^{-3}, 10^{-3}, 2.5×10^{-3}, 5×10^{-3}, 7.5×10^{-3}, 10^{-2}, units in meters, and 10^1, 10^2, 10^3, 10^4, 10^5, 10^6 for σ_1 and μ_1, respectively, assuming $\mu_1 = \mu_2$ and a value of 5×10^{-4} m for σ_2. The latter leads to a contribution of injection test data of 30% of the total objective function. The best values of σ_1 and μ_1 were 5×10^{-3} m and 10^3, respectively. This value of μ_1 (and of μ_2), the third smallest among the tested set, gives little importance to prior information of parameters (10% of the total objective function), which confirms the large uncertainty of the old hydraulic tests data. Thus, we allow large departures of model parameters from their prior estimates.

Estimated $\log_{10} T$ fields (Figure 4) identify preferential flowpaths defining the hydraulic connectivity structure and compare well to those revealed by the "as-built"

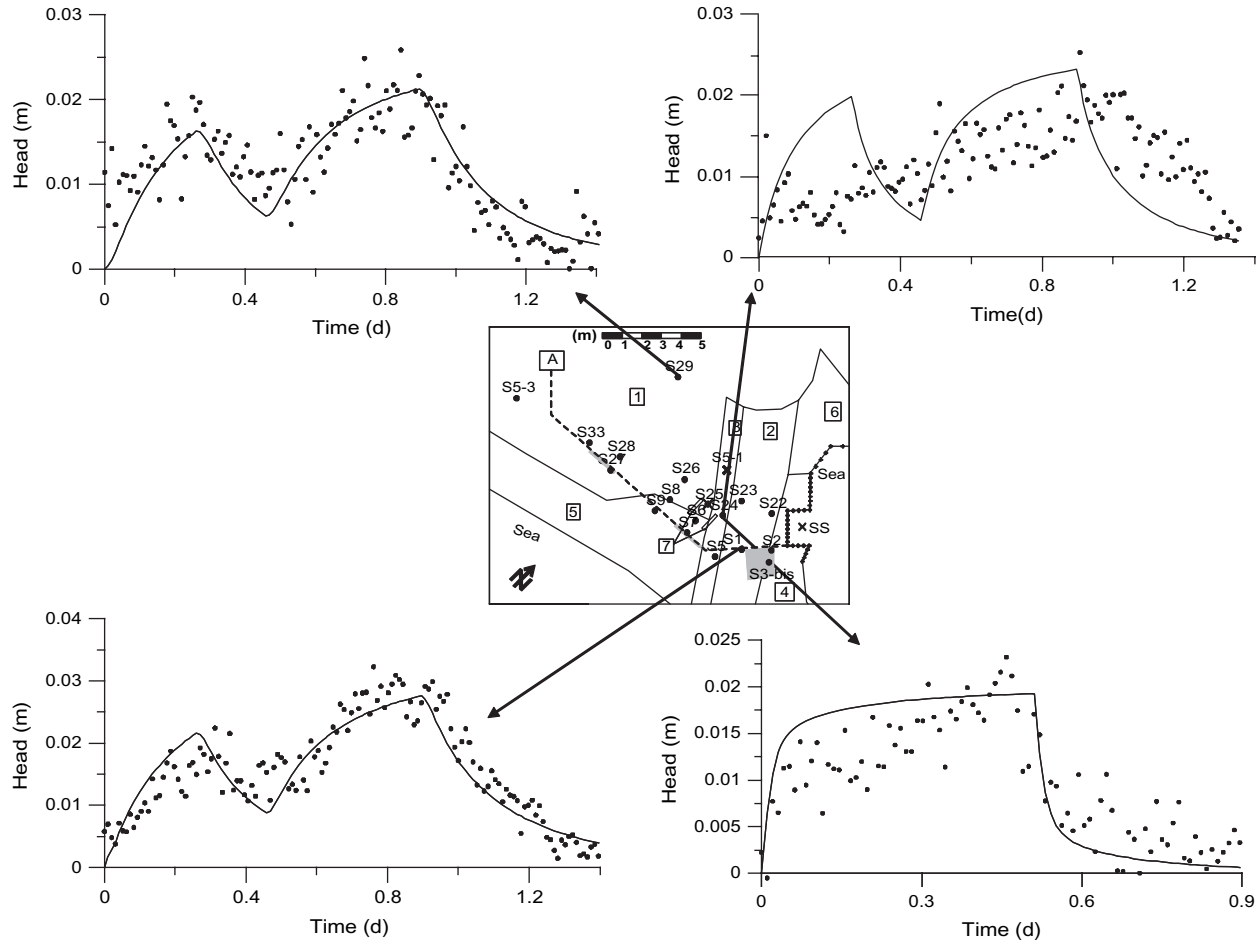

Figure 6. Calculated (line) and measured (circles) response to injections at boreholes S5-1 (boreholes S24—on top right, S29, and S12-1) and S25 (borehole S24 on bottom right) using $\log_{10} T$ field calibrated by the hydraulic information-based model (Figure 4a).

maps (Figure 1). Unfortunately, this information is rarely available but becomes a valuable tool for the verification of our methodology. As expected, these flowpaths are defined by the zones of the sea water pipeline and its filling (zones 2 and 3 in Figure 1, respectively). The similarity of $\log_{10} T$ fields is an important finding of this study. The hydraulic information-based model is capable of reproducing the "anthropogenic" geological contacts although these were not explicitly accounted for. A quantitative analysis of this similarity was performed. We calculated the mean transmissivity of mesh elements within a zone (Table 6). This operation is straightforward for the geology-based model, as each mesh element has an explicitly assigned zone of transmissivity to which it belongs. This rule (element to zone) has been used for sampling the T field of the hydraulic information-based model (i.e., a unique zone of transmissivity) to calculate mean values of transmissivity for comparison with those obtained by the geology-based model. Mean values of transmissivity are similar in both models. They differ significantly mainly in zones 2 and 3, representing the sea water pipelines and their accommodation. The geology-based model concentrates the largest transmissivities in the sea water pipeline filling, whereas the hydraulic information-based model extends this preferential flowpath to zone 5, depicting tetrapod defences. Mean transmissivities are also different in zone 4, where no hydraulic data are available. As regards storage coefficients of conglomerate base and anthropogenic filling, these were assumed to be constant though unknown (modeled with one pilot point). The estimated values are very similar to the prior information (0.09 vs. 0.1 for the conglomerates and 0.25 vs. 0.3 for the anthropogenic fill).

Fits of measured hydraulic data were very similar and very satisfactory for both models (Figures 5 and 6). The high quality of the match reflects, first, that the model is properly capturing the problem dynamics; second, that high diffusivity leads to a strong aquifer response; and, third, that, as a consequence, using the actual sea-level fluctuations (as opposed to sinusoidal approximations) facilitates taking full advantage of the information contained in the data. Also, in hindsight, it is likely that similar results could have been obtained with much shorter observation period. This observation cannot be generalized. If diffusivity had been much smaller or if observation points had been located much farther inland, short-term (daily) fluctuations would have been filtered out and estimated diffusivities would have been controlled by lower-frequency sea-level fluctuations, so that a long observation period would have been required. Only

Table 5
Summary of Average Residuals (Mean Difference between Calculated and Measured State Variables at a Given Borehole) of the Calibration

	Hydraulic Information Based ($\times 10^{-2}$)	Geology Based ($\times 10^{-2}$)
P1-S5	1.30	1.33
P1-S6	1.17	1.38
P1-S7	1.12	1.25
P1-S9	1.12	1.27
P1-S22	1.65	1.59
P1-S24	1.48	1.52
P1-S25	1.06	1.12
P1-S26	1.73	1.86
P1-S27	1.29	1.31
P1-S29	1.30	1.47
P1-S5-3	1.04	1.04
P2-S12-1	4.96	3.77
P2-S24	5.39	5.00
P2-S25	7.06	6.85
P2-S26	4.15	3.62
P2-S29	4.81	4.91
P3-S24	4.97	3.52

Notes: P1, P2, and P3 denote the flow problems of tidal response and injections at boreholes S5-1 and S25, respectively. For instance, P3-S24 denotes measurements at borehole S24 corresponding to injection at borehole S25.

Table 6
Mean Estimated Transmissivities (m^2/d) in Each Zone of Figure 1 Using the Hydraulic Information-Based and the Geology-Based Models

Model	Hydraulic Information Based	Geology Based
Quaternary conglomerate (zone 1)	3400	2400
Sea water pipelines (zone 2)	8400	23,200
Sea water pipelines filling (zone 3)	4400	24,400
Tetrapod defenses (zone 4)	2000	55
Tetrapod defenses (zone 5)	3600	1500
Tetrapod defenses (zone 6)	4900	3500

the fits obtained using the hydraulic information–based model are presented. Average residuals (mean difference between calculated and measured values at a given observation borehole, Table 5) of tidal response are close to zero in both cases. As expected, the hydraulic information-based model yielded slightly larger average residuals for injections given that the geological zonation was not accounted for explicitly. Surprisingly, hydraulic information-based model yields smaller residuals as regards tidal response.

In addition, several calibrations of $\log_{10} T$ (assuming storage coefficients to be known) using only tidal response data and prior information were performed (i.e., neglecting injection test data). Those runs (beyond the scope of this paper) yielded $\log_{10} T$ fields similar to those depicted in Figure 4 and excellent fits of measured tidal response data. Thus, tidal response data are alone a powerful tool for identifying preferential flowpaths.

As regards transport prediction, predicted concentrations compare well to available concentration measurements (not used in the calibration) as displayed in Figure 7. The fit of concentration measurements is not as good as the one of hydraulic data due to the large uncertainties in the transport model. The use of zonation as hard data (geology-based conceptual model) yielded slightly better predictions.

Conclusions

Tidal response is widely used to obtain point values of hydraulic diffusivity by means of the TRM, which assumes homogeneity. The objective of this study was to overcome this limitation and use the tidal response to identify preferential flowpaths. To this end, we applied an integrated methodology, which ranges from data gathering and filtering to geostatistical inversion. Spatial variability of transmissivity and storage coefficient is characterized using the regularized pilot points method. The procedure demands the joint calibration of tidal response and injection test data, which allows us to resolve diffusivity into transmissivity and storage coefficient.

This methodology is applied to a contaminated artificial coastal fill. The construction project revealed the location of several zones of anthropogenic heterogeneity. To validate the methodology, we tested two model structures. Information about anthropogenic zonation was ignored at first ("hydraulic information-based model"), but included in the second structure, termed "geology-based model." Results are summarized as follows:

1. The flowpaths identified by the hydraulic information-based model are consistent with those revealed by the "as-built" maps. This lends support to the robustness of the methodology.
2. The hydraulic information-based model is capable of identifying the anthropogenic zonation, which was accounted for only in the geology-based model. This may be of great help for identifying contacts between different "geological" formations.
3. Excellent fits of measured tidal responses and good fits of injection test data were obtained with both model structures. Joint calibration of the two sets of data (tidal responses and injection tests) requires assessing the relative weight given to each data set and, in general, increasing modeling efforts. However, we believe the added model reliability is worth the effort.
4. Calculated concentrations of a transport prediction compare well with the observed ones.

We conclude that tidal response is a useful and economical tool for identifying preferential flowpaths in coastal aquifers, and that the presented methodology, which includes the regularized pilot points method is, indeed, robust. As such, it can be used for coastal aquifer

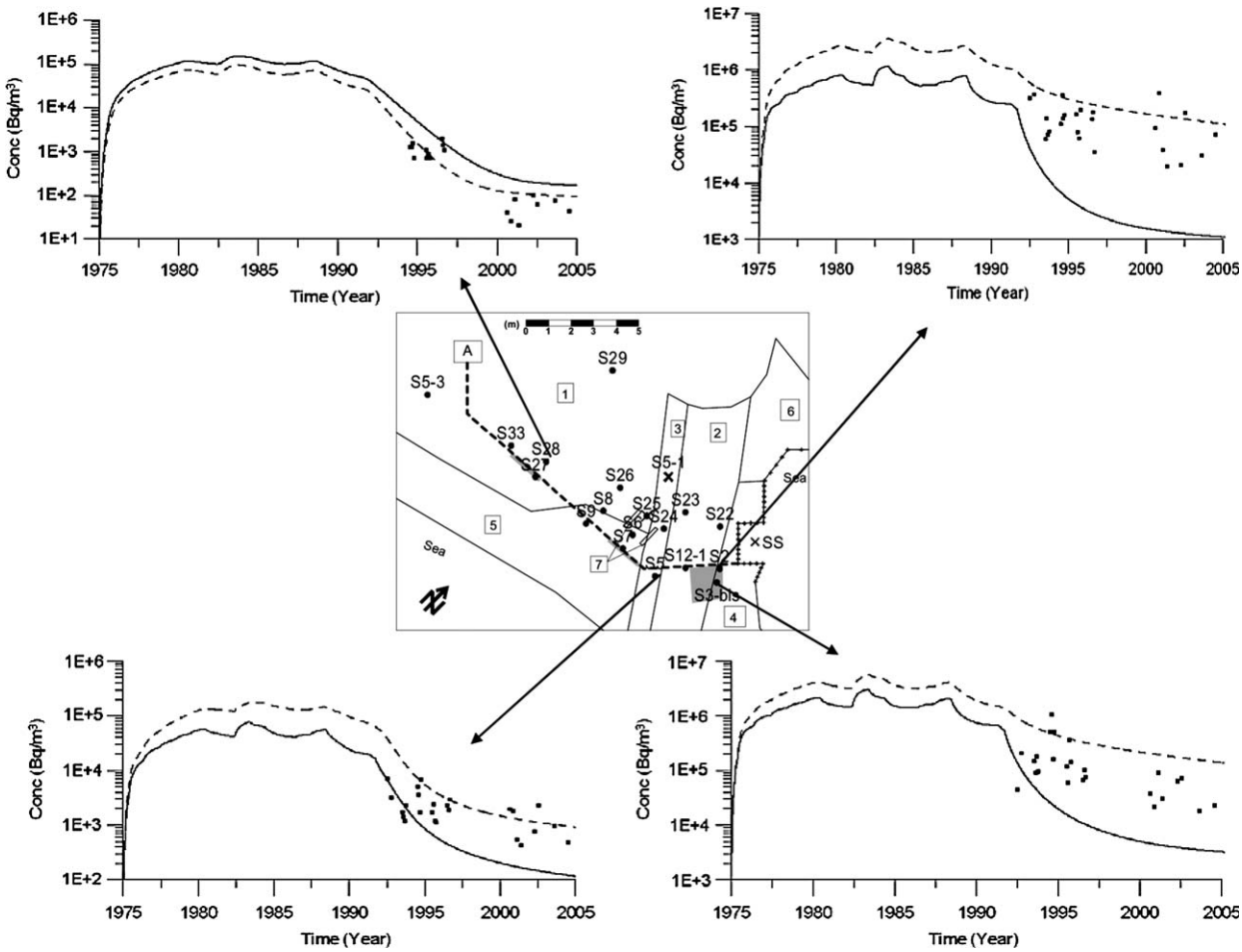

Figure 7. Measured (dots) and calculated concentrations obtained with the geology-based model (continuous line) and the hydraulic information-based (dashed line) models.

management whenever identification of connectivity patterns is important. This includes the design of measures to control sea water intrusion (Abarca et al. 2006).

Acknowledgments

This study was funded by ENRESA (Spanish Agency for Nuclear Waste Disposal) and MEC (Spanish Ministry for Education and Science). The authors gratefully acknowledge the comments and suggestions of three anonymous reviewers.

References

Abarca E., E. Vazquez-Sune, J. Carrera, B. Capino, D. Gamez, and F. Batlle. 2006. Optimal design of measures to correct seawater intrusion. *Water Resources Research* 42, no. 9: Art. No. W09415.

Alcolea A., J. Carrera, and A. Medina. 2006a. Pilot points method incorporating prior information for solving the groundwater flow inverse problem. *Advances in Water Resources* 29, no. 11: 1678–1689.

Alcolea A., J. Carrera, and A. Medina. 2006b. Inversion of heterogeneous parabolic-type equations using the pilot points method. *International Journal for Numerical Methods in Fluids* 51, no. 9–10: 963–980.

Bea S.A., J. Carrera, J.M. Soler, C. Ayora, and M. Saaltink. 2004. Simulation of remediation alternatives for a Cs-137 contaminated soil. *Radiochimica Acta* 92, no. 9–11: 827–833.

Carrera J., and S.P. Neuman. 1986a. Estimation of aquifer parameters under transient and steady-state conditions, 1. Maximum likelihood method incorporating prior information. *Water Resources Research* 22, no. 2: 199–210.

Carrera J., and S.P. Neuman. 1986b. Estimation of aquifer parameters under transient and steady-state conditions, 2. Uniqueness, stability and solution algorithms. *Water Resources Research* 22, no. 2: 211–227.

Carrera J., and S.P. Neuman. 1986c. Estimation of aquifer parameters under transient and steady-state conditions, 3. Applications. *Water Resources Research* 22, no. 2: 228–242.

Chapuis R.P., C. Belanger, and D. Chenaf. 2006. Pumping test in a confined aquifer under tidal influence. *Ground Water* 44, no. 2: 300–305.

Chen C., and J.J. Jiao. 1999. Numerical simulation of pumping tests in multilayer wells with non-Darcian flow in the wellbore. *Ground Water* 37, no. 3: 465–474.

Drogue C., M. Razack, and P. Krivic. 1984. Survey of a coastal karstic aquifer by analysis of the effect on the sea-tide: Example of the Kras of Slovenia, Yugoslavia. *Environmental Geologic Water Sciences* 6, no. 2: 103–109.

Erskine A.D. 1991. The effect of tidal fluctuation on a coastal aquifer in the UK. *Ground Water* 29, no. 4: 556–562.

Fakir Y. 2003. Hydrodynamic characterization of a Sahelian coastal aquifer using the ocean tide effect (Dridrate Aquifer, Morocco). *Hydrological Sciences Journal* 48, no. 3: 441–454.

Ferris J.G. 1951. Cyclic fluctuations of water level as a basis for determining aquifer transmissibility. In *International Association of Hydrological Sciences*, Publication 33, vol. 2, 148–155. Wallingford, U.K.: IAHS.

Hvorslev M.J. 1951. Time-lag and soil permeability in groundwater observations. Bulletin 36. Vicksburg, Mississippi:

US Army Corps of Engineers, Waterways Experiment Station.
Jhan M.K., Y. Kamii, and K. Chikamori. 2003. On the estimation of phreatic aquifer parameters by the tidal response technique. *Water Resources Management* 17, no. 1: 69–88.
Knudby C., and J. Carrera. 2005. On the relationship between indicators of geostatistical, flow and transport connectivity. *Advances in Water Resources* 28, no. 4: 405–421.
Li H.L., and J.J. Jiao. 2001. Analytical studies of groundwater-head fluctuation in a coastal confined aquifer overlain by a semi-permeable layer with storage. *Advances in Water Resources* 24, no. 5: 565–573.
Li H.L., J.J. Jiao, M. Luk, and K.Y. Cheung. 2002. Tide-induced groundwater level fluctuation in coastal aquifers bounded by L-shaped coastlines. *Water Resources Research* 38, no. 3: paper 1024.
Medina A., and J. Carrera. 2003. Geostatistical inversion of coupled problems: Dealing with computational burden and different types of data. *Journal of Hydrology* 281, no. 4: 251–264.
Meier P., A. Medina, and J. Carrera. 2001. Geostatistical inversion of Cross-Hole pumping tests for identifying preferential flow channels within a shear zone. *Ground Water* 39, no. 1: 10–17.
Meier P., J. Carrera, and X. Sanchez-Vila. 1998. An evaluation of Jacob's method work for the interpretation of pumping tests in heterogeneous formations. *Water Resources Research* 34, no. 5: 1011–1025.
Millham N.P., and B.L. Howes. 1995. A comparison of methods to determine K in shallow coastal aquifer. *Ground Water* 33, no. 1: 49–57.
Pandit A., C.C. Elkhazen, and S.P. Sivaramapillai. 1991. Estimation of hydraulic conductivity values in a coastal aquifer. *Ground Water* 29, no. 2: 175–180.
Rötting T., J. Carrera, J. Bolzicco, and J.M. Salvany. 2006. Stream-stage response tests and their joint interpretation with pumping tests. *Ground Water* 44, no. 3: 371–385.
Schultz G., and C. Ruppel. 2002. Constraints on hydraulic parameters and implications for groundwater flux across the upland-estuary interface. *Journal of Hydrology* 260, no. 1–4: 255–269.
Shih D.C.F., and G.F. Lin. 2004. Application of spectral analysis to determine hydraulic diffusivity of a sandy aquifer (Ping-Tung County, Taiwan). *Hydrological processes* 18, no. 9: 1655–1669.
Trefry M.G. 1999. Periodic forcing in composite aquifers. *Advances in Water Resources* 22, no. 6: 645–656.
Trefry M.G., and E. Bekele. 2004. Structural characterization of an island aquifer via tidal methods. *Water Resources Research* 40, no. 1: W01505.
Trefry M.G., and C.D. Johnston. 1998. Pumping test analysis for a tidally forced aquifer. *Ground Water* 36, no. 3: 427–433.
UPC. 2002. Ephebo 1.1 rev 2. Estimación de parámetros hidráulicos mediante ensayos de bombeo. Hydrogeology Group. Department of Geotechnical Engineering and Geosciences. http://www.h2ogeo.upc.es/English/software.htm.
Wang J., and T.K. Tsay. 2001. Tidal effects on groundwater motions. *Transport in Porous Media* 43, no. 1: 159–178.
Weiss R., and L. Smith. 1998. Parameter space methods in joint parameter estimation for groundwater flow models. *Water Resources Research* 34, no. 4: 647–661.

Appendix

Kriging with External Drift for Reconstructing Heads at a Borehole

Time evolution of heads at boreholes affected by tidal fluctuations exhibits a marked nonstationary behavior. These data can be modeled as the sum of a deterministic drift [heads at a reference borehole in this case, $h^{\text{ref}}(t)$] and a stochastic component $\varepsilon(t)$, which is an intrinsic random function with zero mean and known variogram $\gamma_\varepsilon(t)$. Imposing unbiasedness constraints and minimizing the error variance leads to the system of equations of kriging with external drift:

$$\sum_{j=1}^{N} \gamma_\varepsilon(t_i - t_j)\lambda_j + \mu_1 + \mu_2 h^{\text{ref}}(t_i) = \gamma_\varepsilon(t_i - t) \quad i = 1, \ldots, N \tag{A1}$$

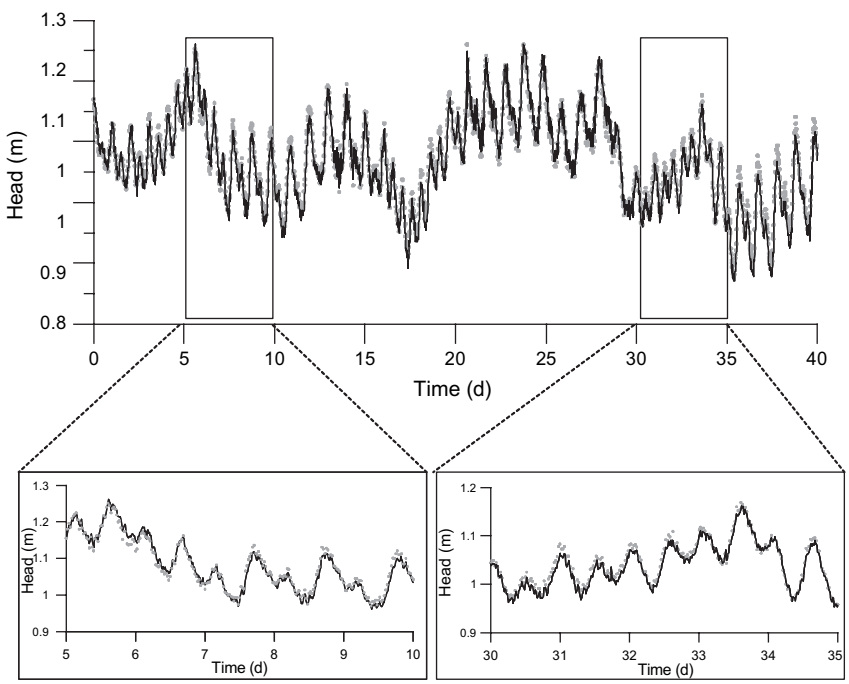

Figure A1. Measured (circles) and reconstructed (line) tidal response at borehole S5 using S9 measurements as external drift.

$$\sum_{j=1}^{N} \lambda_j = 1 \tag{A2}$$

$$\sum_{j=1}^{N} \lambda_j h^{\mathrm{ref}}(t_j) = h^{\mathrm{ref}}(t_j) \tag{A3}$$

This system is solved for the N kriging weights λ (corresponding to N head measurements) and for μ_1, μ_2 (Lagrange multipliers of the constraints A2 and A3), at each time where $\varepsilon(t)$ is estimated. Cross-validation was performed to select the variogram $\gamma_\varepsilon(t)$ and to test the statistical significance of the estimation. Optimum results were obtained with a monomic model ($\gamma_\varepsilon = kt^\theta$; $k = 0.12$; $\theta = 0.04$). Mean error (which should be close to zero) was 0.0954 and dimensionless mean quadratic error (which should be close to one) was 1.044. In addition, the selected variogram was validated by estimating heads at reference borehole S5, where all measurements were available. Measured heads at reference borehole S9 were used as external drift (Figure A1).